ACS Macro Letters

Letter

Cite This: ACS Macro Lett. 2018, 7, 1480−1485

pubs.acs.org/macroletters

Hydrothermal Synthesis of Composition- and Morphology-Tunable Polyimide-Based Microparticles

Taehyung Kim,[†,⊥] Byeongho Park,[‡,⊥] Kyung Min Lee,[†] Se Hun Joo,[†] Min Seok Kang,[§] Won Cheol Yoo,[§] Sang Kyu Kwak,*[,†] and Byeong-Su Kim*[,∥]

[†]Department of Energy Engineering, School of Energy and Chemical Engineering, Ulsan National Institute of Science and Technology (UNIST), 50 UNIST-gil, Ulsan 44919, Republic of Korea

[‡]Composites Research Division, Korea Institute of Materials Science, 797 Changwon-daero, Changwon 51508, Republic of Korea

[§]Department of Chemical & Molecular Engineering and Applied Chemistry, Hanyang University, Ansan, Gyeonggi-do 15588, Republic of Korea

[∥]Department of Chemistry, Yonsei University, Seoul 03722, Republic of Korea

Supporting Information

ABSTRACT: Polyimide is one of the most important high-performance polymers, which is widely used due to its excellent mechanical performance and thermal stability. Unlike the conventional synthetic approach, hydrothermal polymerization enables the synthesis of polyimides without any toxic solvent and catalyst. Herein, we report the synthesis of polyimide-based microparticles (PIMs) through one-pot hydrothermal polymerization using precursors of mellitic acid (MA) and three isomers of phenylenediamine (PDA) (*o*-, *m*-, and *p*-PDA). Interestingly, the chemical composition of PIMs was highly tunable with the choice of the PDA isomers, leading to considerable morphological differences between PIMs. The molecular dynamics simulation and density functional theory calculation of the polymeric segment of the respective PIMs suggested that the relative ratio of amide to imide influenced the rotational freedom of the polymeric chains and number of hydrogen bonds, resulting in the well-defined structures of respective PIMs. Considering the highly tunable nature of PIMs coupled with the facile synthetic protocol, we anticipate prospective potentials of PIMs in materials, energy, and composite applications.

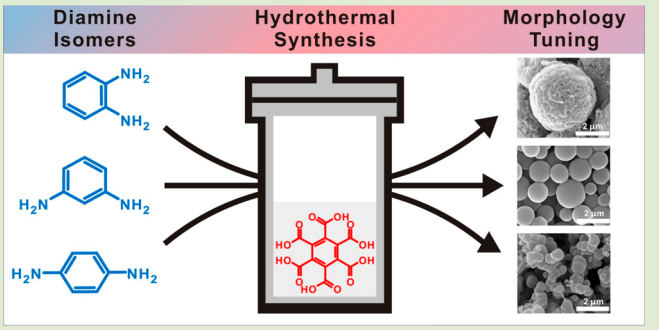

Polyimide (PI) is one of the most important high-performance polymers with excellent thermal stability, mechanical performance, and chemical resistance.[1] The classical synthesis of PI involves a condensation reaction between aromatic dianhydrides and aromatic diamines under high-boiling and toxic solvents, catalysts, and high temperatures, which often imposes technical challenges in practical applications.[2−4] The formation of PI from its building block is essentially irreversible, and often, its chemical stability makes the PI neither soluble nor fusible with other materials. Therefore, two-step casting and imidizing of the polyamic acid intermediate are necessary for the applications of PIs.[5,6] Consequently, in situ control over its composition, crystallinity, and morphology can provide a new means to create PIs with advanced material properties.

As an alternative to the conventional method, recent progresses are geared toward alleviating many synthetic challenges, including (1) phase separation of poly(amic acid) oligomers in apolar solvents,[7] (2) the polymerization of dianhydrides and diisocyanates via decarboxylation,[8] (3) solvent-free, solid-state polymerization,[9] (4) polymerization in ionic liquids as reaction media,[10] and (5) hydrothermal polymerization.[11] In particular, hydrothermal polymerization is a high-temperature, high-pressure aqueous solution reaction that has been explored due to its simplicity, environmental sustainability, and low cost.[12] The hydrothermal reaction has been typically employed in the synthesis of inorganic crystalline materials such as zeolites and carbonaceous materials.[13] As a notable example, Unterlass and co-workers have recently employed hydrothermal polymerization for the synthesis of poly(*p*-phenylene pyromellitimide) with high crystallinity.[11] The growth mechanism of highly crystalline poly(*p*-phenylene pyromellitimide) was attributed to the repeated dissolution−polymerization−crystallization of monomer salts.

With the advancement of synthetic approaches, a fine control over the morphology and molecular orientation in PI synthesis is increasingly receiving attention owing to its

Received: September 7, 2018
Accepted: November 28, 2018

DOI: 10.1021/acsmacrolett.8b00680
ACS Macro Lett. 2018, 7, 1480−1485

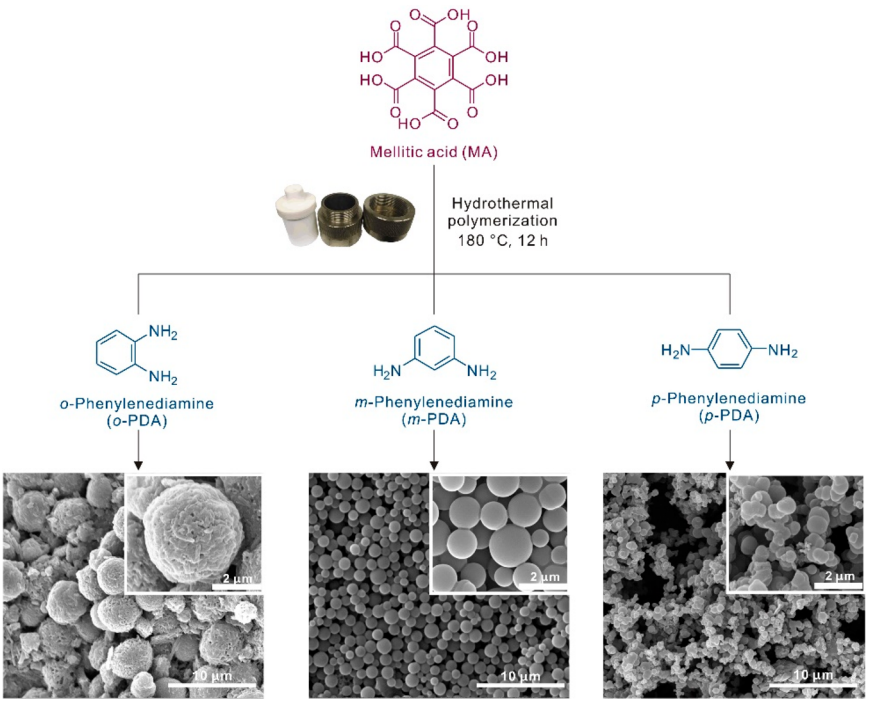

Figure 1. Schematic representation of hydrothermal polymerization of mellitic acid (MA) and three structural isomers of phenylenediamine (*o*-, *m*-, and *p*-PDA) and the corresponding SEM images of the polyimide-based microparticles (PIMs).

significant influence on the mechanical and chemical stability. For example, PI particles have been typically synthesized by precipitation due to its poor solubility and intractability. Kimura and co-workers have reported the control over the morphology of PI in various structures such as nanoribbon, whisker, and sphere through a reaction-induced phase separation during the solution polymerization process.[14−16] Even with the progress in the morphology control of PI structures, the critical role of the precursors in controlling the chemical structures of PIs with different macroscopic morphology has not been a subject of intensive study.

Herein, we report a one-pot hydrothermal polymerization of polyimide-based microparticles (PIMs) from the condensation between mellitic acid (MA) and three structural isomers of phenylenediamine (PDA) (e.g., *o*-, *m*-, and *p*-PDA) without the formation of monomer salts. We found that the chemical composition of PIMs was highly tunable with the choice of PDA isomers, leading to a fine control over the morphology of PIMs with varying dimension. These structural isomers of PDA influenced the mode of hydrothermal polymerization owing to the different structural requirement and rotational freedom of the polymeric chains, which eventually determined the characteristics of PIM such as the chemical resistance and thermal stability.

As illustrated in Figure 1, three types of PIMs were synthesized by the condensation reaction of the amine group of PDA and carboxylic acid of MA through hydrothermal polymerization at 180 °C for 12 h. Unlike the conventional bifunctional pyromellitic dianhydride monomers, here we choose multifunctional mellitic acid as a precursor to allow the condensation reactions with isomers of phenylenediamines to control the composition and morphology of nano- and microstructures of polymeric particles. The molar ratio between PDA and MA was fixed to three, to balance the number of amine and carboxylic acid functional groups (see Supporting Information for details). Although the condensation reaction between amine and carboxylic acid groups does not readily occur without a proper catalyst, it is reported that the imide formation between them becomes favorable at hydrothermal condition.[17]

Interestingly, the morphology of the resulting PIMs was considerably different for different PDAs (Figure 1). For example, no uniform morphology was observed in the case of *o*-PIMs and *p*-PIMs, while *m*-PIMs displayed micrometer-sized particles with a regular spherical shape. The average diameter of *m*-PIMs was determined to be 1.12 ± 0.33 μm with a relatively low size distribution. We also explored the effect of solution concentration on the particle size by varying the concentration of *m*-PDA and MA from 1.0 to 20 mg/mL (Figure S1 in the Supporting Information). The average particle diameter of *m*-PIMs increased gradually from 0.74 to 1.25 μm, while their spherical morphology remained constant regardless of the reaction conditions. In order to further investigate the composition and morphological changes depending on the reaction time and relative ratio of PDA to MA during the hydrothermal polymerization, *m*-PIMs were synthesized by varying reaction time from 24 to 48 h and the molar ratio of PDA to MA from 1.5 to 6 with the overall concentration of *m*-PDA and MA fixed at 10 mg/mL. Although the reaction time increased, the morphology, thermal stability, and chemical compositions were not significantly affected by the longer reaction time (Figure S2). In addition, when different precursor ratios are employed, all *m*-PIMs displayed a spherical morphology with a similar composition and thermal stability (Figure S3).

The chemical structures of the respective PIMs were characterized on the basis of FT-IR and X-ray photoelectron spectroscopy (XPS) (Figure 2). The deconvoluted spectrum of the overlapped FT-IR peaks clearly suggested the presence of an aromatic group, carbonyl groups from amide/carboxylic

DOI: 10.1021/acsmacrolett.8b00680
ACS Macro Lett. 2018, 7, 1480−1485

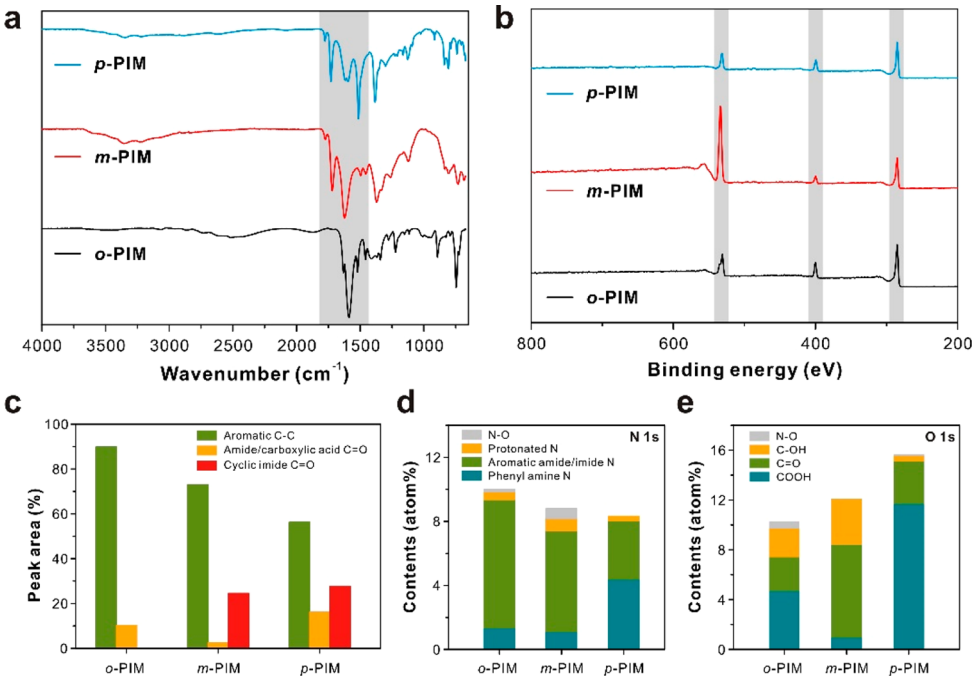

Figure 2. (a) FT-IR spectra and (b) X-ray photoelectron spectroscopy (XPS) survey spectra of respective PIMs prepared from different precursors. (c) Relative ratio of respective peak areas based on FT-IR spectra and (d, e) comparison of the deconvoluted high-resolution spectrum of *o*-, *m*-, and *p*-PIM in (d) N 1s and (e) O 1s peaks combined with elemental analysis.

acid and from cyclic imide in the region of 1450−1800 cm^{-1}. Interestingly, *o*-PIMs displayed no peaks over 1700 cm^{-1} corresponding to cyclic imide, mainly due to the restricted steric requirement for the formation of cyclic imide between the carbonyl groups and two neighboring amine groups at the ortho-position. Unlike the *o*-PIMs, both *m*- and *p*-PIMs showed symmetric and asymmetric carbonyl peaks of cyclic imide at 1710−1730 and 1775 cm^{-1}, respectively (Figure S4). The relative fraction of the respective functional groups was compared by the deconvoluted peak area. The fraction of the imide group was similar in both *m*- and *p*-PIMs, at 25% and 28%, respectively. However, the fraction of the amide group was considerably different, at 2.5% and 16% for *m*-PIMs and *p*-PIMs, respectively. This result clearly demonstrates the critical role of precursors in controlling the chemical structures of PIMs with different macroscopic morphology.

The chemical composition and the states of the respective elements in the PIMs were further investigated by elemental analysis (EA) coupled with XPS (Figure 2 and Table S1). The EA data suggested that there was almost no difference in the fraction of carbon within the respective PIMs (ca. 47%). Interestingly, however, the fraction of nitrogen and oxygen varied considerably depending on the type of PIMs; for example, there was 10.0, 8.8, and 8.3% of nitrogen and 10.3, 12.1, and 15.7% of oxygen for *o*-PIM, *m*-PIM, and *p*-PIM, respectively. Furthermore, by combining the elemental composition analysis with the deconvoluted high-resolution XPS spectra, each element comprising the PIMs was carefully assigned. For example, the C 1s spectra revealed the presence of four distinct components, including sp^2 carbon (284.4 eV), C−N group (285.5 eV), amide group (287.4 eV), and imide group (288.8 eV), which are all in good agreement with the previous report (Figure S5).[18] In addition, the N 1s spectra demonstrated the peaks attributable to amide (398.8 eV), aromatic imide (399.8 eV), and protonated N (401.3 eV) (Figure 2d).[19,20] Similarly, the O 1s peaks were assigned to carboxylic acid (531.2 eV), carbonyl (533.0 eV), and hydroxyl (535.0 eV) (Figure 2e).[21] For nitrogen, the atomic percentage of the aromatic amide and imide bond was decreased from *o*-PIM to *p*-PIM as the fraction of the C−N bond also decreased. Taken together, these data again indicated that not only the morphology but also the chemical composition of the respective PIMs were distinct with the type of precursors for the hydrothermal polymerization.

Because of the different chemical compositions, particularly the ratio of the imide to amide bond, the PIMs displayed a different chemical resistance in solvents (Figure S6 and Table S2). For instance, *o*-PIM having only amide bonds dissolved readily in polar solvents such as DMF, DMSO, and NMP, whereas *m*-PIM with a high fraction of the imide group does not indicate any solubility in the solvent tested except a partial solubility in DMSO. This observation clearly demonstrates the important role of the imide bond for enhanced chemical resistance in PIMs. Moreover, the thermogravimetric analysis (TGA) revealed the thermal stability of the PIMs (Figure S7). The first critical weight loss occurred at 9.5%, 7.9%, and 13.3% at 240, 250, and 340 °C for *o*-PIM, *m*-PIM, and *p*-PIM, respectively, which indicated the transition of amide to imide bonds in accord with the portion of amide bonds present in the FT-IR data (Figure S4 and Table S3). Even though the fraction of imide increases, there were still amide bonds remaining which indicated that the conversion of the amide to imide bond did not reach 100%. The weight percentage of the residues after thermal decomposition at 600 °C was 59.6%, 66.1%, and 49.1%, respectively. Interestingly, both *m*-PIM and *p*-PIM maintained their spherical structure even after annealing at 900 °C, while *o*-PIM melted and lost its structural integrity even at 500 °C, suggesting a critical role of the imide group for enhanced thermal stability (Figures S8 and S9). Although the amount of remaining residues after annealing at 1000 °C was

DOI: 10.1021/acsmacrolett.8b00680
ACS Macro Lett. 2018, 7, 1480−1485

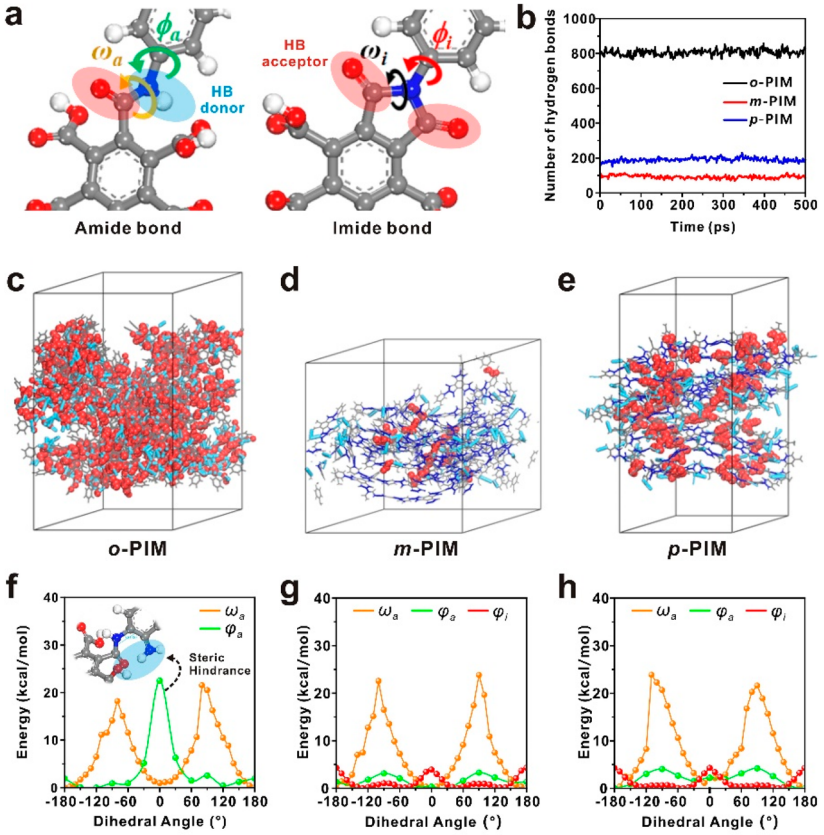

Figure 3. (a) Chemical and structural differences between amide and imide bonds. (b) Time evolution of the number of hydrogen bonds of *o*-, *m*-, and *p*-PIMs. (c–e) MD snapshots of (c) *o*-, (d) *m*-, and (e) *p*-PIMs. Water molecules are not shown for clarity. Atoms constituting amide bonds and imide bonds are red and blue, respectively. Hydrogen bonds are displayed as sky-blue colored sticks. (f–h) DFT-based potential energy profiles for the ω_a, φ_a, and φ_i in (f) *o*-, (g) *m*-, and (h) *p*-PIMs.

smaller than that of commercial PI (PMDA-ODA)[22] due to amide to imide transition, the weight loss at 600 °C was similar, indicating a comparable thermal stability with commercial PI. Moreover, the high solubility of *o*-PIM together with the low thermal stability indicates a low molecular weight oligomeric structure of *o*-PIM, which was additionally supported by the ESI-MS (Figure S10). The sharp X-ray diffraction peaks of *o*-PIMs and *p*-PIMs indicated a crystalline nature. However, *m*-PIM displayed an amorphous structure with a broad peak (Figure S11). We attributed this amorphous nature of *m*-PIM to the uncontrolled imide and amide bond formation of MA as a carboxylic acid precursor in contrast to the high crystallinity obtained by the hydrothermal polymerization of pyromellitic acid dianhydride as reported previously.[10]

These morphological distinctions between the PIMs are attributed to the direction of amine groups in the PDA isomers. Specifically, the differences in amine group orientation are considered to influence the formation of the cyclic imide bond of PIMs due to steric hindrance when PDA reacts with the six potential reaction sites of MA. Moreover, as the hydrothermal polymerization proceeded, the population of polar groups such as carboxylic acid and amine groups was reduced; thus, the polymerization intermediates (e.g., oligomers of PIM) would possess a difference in the aqueous solubility, causing phase separation during the growth. During this phase separation, the PIMs prefer a spherical morphology that minimizes the surface area, to be thermodynamically stable. Here, we noted two chemical structural differences between amide and imide bonds as the main factors that can influence the morphology of the resulting PIMs: hydrogen bond and rotation of C–N bond (Figure 3a).

In order to gain an in-depth understanding of the hydrogen bonding interactions of PIMs, we performed all-atom molecular dynamics (MD) simulations of *o*-, *m*-, and *p*-PIMs under hydrothermal conditions (see computational details in the Supporting Information, Figure S12 and Table S4). Within the PIMs, an amide bond has one hydrogen bonding donor and one hydrogen bonding acceptor, whereas an imide bond has two hydrogen bonding acceptors without donor (Figure 3a). As expected from the chemical structure of the amide bond with the donor–acceptor pair, the PIM with a higher amide group ratio forms more hydrogen bonds; the number of hydrogen bonds of PIM (i.e., a total of the inter- and intramolecular hydrogen bonds of PIM molecules) was calculated to be the highest for *o*-PIM (806), followed by *p*-PIMs (208) and *m*-PIM (92) (Figure 3b). Also, it is noteworthy that amide bonds tended to be aggregated with each other because they form intramolecular hydrogen bonds (red spheres in Figure 3c–e), while imide bonds did not show any tendency to form a condensed structure. Since they only contain hydrogen bonding acceptors, aggregation did not occur as much as amide bonds. With this result, it is expected that self-aggregation of *o*-PIM molecules can induce the rough surface of *o*-PIM through abundant hydrogen bonds, while surfaces of *m*- and *p*-PIMs are relatively smooth.

To investigate the rotational behavior of C–N bonds in PIMs, we systematically compared the energy barrier for the

DOI: 10.1021/acsmacrolett.8b00680
ACS Macro Lett. 2018, 7, 1480–1485

rotation through the density functional theory (DFT) calculations (see computational details in the Supporting Information). Here, we considered all C−N bonds between monomers (ω_a and φ_a for amide bond and ω_i and φ_i for imide bond in Figure 3a) and compared ω_a with ω_i and φ_a with φ_i, where C−N bonds with the similar local structures corresponded to each other. Note that we calculated the potential energy profiles only for ω_a, φ_a, and φ_i since the rotation of ω_i was restricted by covalent bonds. Regardless of the *o*-, *m*-, and *p*-PIMs, both ω_a and ω_i were difficult to rotate due to the high energy barrier (>23 kcal mol^{-1}) for ω_a (orange lines in Figure 3f−h) and the strong covalent bond for ω_i. In the case of φ_a and φ_i, the energy required for the free rotation depends on the types of PIMs (i.e., *o*-, *m*-, and *p*-PIM). For φ_a and φ_i in *m*- and *p*-PIMs, the energy barriers were low (∼4 kcal mol^{-1}), and thus C−N bonds were expected to rotate; however, the difference between them is negligible (red and green lines in Figure 3g and 3h). On the other hand, a noticeable difference was observed for φ_a in *o*-PIM, which showed the high energy barrier (∼23 kcal mol^{-1}) comparable to the ω_a, due to the steric hindrance between the amide bond and the adjacent amine group (green line in Figure 3f). In addition to the hydrogen bonding interactions, this low bond flexibility of *o*-PIM is expected to contribute to the rough surface of *o*-PIM to some extent.

In this report, we synthesized composition- and morphology-tunable polyimide-based microparticles (PIMs) by the hydrothermal method using mellitic acid and isomers of phenylenediamine. The chemical composition of PIMs was highly tunable with the choice of the phenylenediamine isomers, leading to considerable morphological differences between PIMs. Finally, the formation mechanism of the PIMs by the combined molecular dynamics simulation and density functional theory calculation suggested the relative ratio of amide to imide bonds in each PIM, and the possibility of C−N bond rotation influenced the rotational freedom of the polymeric chains, resulting in the well-defined structures of respective PIMs.

■ ASSOCIATED CONTENT

Supporting Information

The Supporting Information is available free of charge on the ACS Publications website at DOI: 10.1021/acsmacrolett.8b00680.

Experimental procedures and characterization data of SEM, FT-IR, XPS, EA, solubility test, TGA, XRD, and MD and DFT calculations (PDF)

■ AUTHOR INFORMATION

Corresponding Authors

*E-mail: bskim19@yonsei.ac.kr.

*E-mail: skkwak@unist.ac.kr.

ORCID

Taehyung Kim: 0000-0003-4518-335X

Byeongho Park: 0000-0001-5884-9793

Se Hun Joo: 0000-0003-4507-150X

Won Cheol Yoo: 0000-0002-4450-9744

Sang Kyu Kwak: 0000-0002-0332-1534

Byeong-Su Kim: 0000-0002-6419-3054

Author Contributions

⊥These authors contributed equally.

Notes

The authors declare no competing financial interest.

■ ACKNOWLEDGMENTS

This work was supported by the National Research Foundation of Korea (NRF-2017R1A2B3012148 and NRF-2016H1D5A1910285), and S.K.K. acknowledges the computational resources from UNIST-HPC.

■ REFERENCES

(1) Hergenrother, P. M. The Use, Design, Synthesis, and Properties of High Performance/High Temperature Polymers: An Overview. *High Perform. Polym.* **2003**, *15*, 3−45.

(2) Liu, Y.-W.; Huang, J.; Tan, J.; Zeng, Y.; Ding, Q.; Xiang, X.; Liu, Y.; Zhang, H. Synthesis and Characterization of Intrinsic High-Barrier Polyimide Derived from a Novel Diamine Monomer Containing Rigid Planar Moiety. *J. Polym. Sci., Part A: Polym. Chem.* **2017**, *55*, 2373−2382.

(3) Yao, H.; Zhang, N.; Shen, K.; Song, N.; Shi, K.; Zhu, S.; Zhang, Y.; Guan, S. From a Flexible Hyperbranched Polyimide to a Microporous Polyimide Network: Microporous Architecture and Carbon Dioxide Adsorption. *Polymer* **2017**, *115*, 176−183.

(4) Xiao, S.; Huang, R. Y. M.; Feng, X. Synthetic 6FDA-ODA Copolyimide Membranes for Gas Separation and Pervaporation: Functional Groups and Separation Properties. *Polymer* **2007**, *48*, 5355−5368.

(5) Oishi, Y.; Itoya, K.; Kakimoto, M.; Imai, Y. Preparation and Properties of Molecular Composite Films of Block Copolyimides Based on Rigid Rod and Semi-Flexible Segments. *Polym. J.* **1989**, *21*, 771−780.

(6) Numata, S.; Oohara, S.; Fujisaki, K.; Imaizumi, J.; Kinjo, N. Thermal Expansion Behavior of Various Aromatic Polyimides. *J. Appl. Polym. Sci.* **1986**, *31*, 101−110.

(7) Wakabayashi, K.; Kohama, S.; Yamazaki, S.; Kimura, K. Morphology Control of Various Aromatic Polyimides by Using Phase Separation during Polymerization. *Polymer* **2007**, *48*, 458−466.

(8) Liaw, D.-J.; Wang, K.-L.; Huang, Y.-C.; Lee, K.-R.; Lai, J.-Y.; Ha, C.-S. Advanced Polyimide Materials: Syntheses, Physical Properties and Applications. *Prog. Polym. Sci.* **2012**, *37*, 907−974.

(9) Unterlass, M. M.; Emmerling, F.; Antonietti, M.; Weber, J. From Dense Monomer Salt Crystals to CO_2 Selective Microporous Polyimides via Solid-State Polymerization. *Chem. Commun.* **2014**, *50*, 430−432.

(10) Vygodskii, Y. S.; Lozinskaya, E. I.; Shaplov, A. S. Ionic Liquids as Novel Reaction Media for the Synthesis of Condensation Polymers. *Macromol. Rapid Commun.* **2002**, *23*, 676−680.

(11) Baumgartner, B.; Bojdys, M. J.; Unterlass, M. M. Geomimetics for Green Polymer Synthesis: Highly Ordered Polyimides via Hydrothermal Techniques. *Polym. Chem.* **2014**, *5*, 3771−3776.

(12) Baumgartner, B.; Puchberger, M.; Unterlass, M. M. Towards a General Understanding of Hydrothermal Polymerization of Polyimides. *Polym. Chem.* **2015**, *6*, 5773−5781.

(13) Cundy, C. S.; Cox, P. A. The Hydrothermal Synthesis of Zeolites: History and Development from the Earliest Days to the Present Time. *Chem. Rev.* **2003**, *103*, 663−702.

(14) Wakabayashi, K.; Uchida, T.; Yamazaki, S.; Kimura, K. Preparation of Poly(4-Phthalimide) Nanoribbon by Reaction-Induced Crystallization. *Macromolecules* **2008**, *41*, 4607−4614.

(15) Kimura, K.; Zhuang, J. H.; Wakabayashi, K.; Yamashita, Y. Morphology Control of Poly(p-Phenylene Pyromelliteimide) by Means of Self-Assembling Polymerization. *Macromolecules* **2003**, *36*, 6292−6294.

(16) Nakayama, H.; Fujitsu, Y.; Uchida, T.; Yamazaki, S.; Kimura, K. Consideration on Formation Mechanism of Aromatic Polyamide Hollow Spheres Prepared by Reaction-Induced Phase Separation. *J. Polym. Sci., Part A: Polym. Chem.* **2015**, *53*, 1966−1974.

DOI: 10.1021/acsmacrolett.8b00680
ACS Macro Lett. 2018, 7, 1480−1485

(17) Baumgartner, B.; Bojdys, M. J.; Skrinjar, P.; Unterlass, M. M. Design Strategies in Hydrothermal Polymerization of Polyimides. *Macromol. Chem. Phys.* **2016**, *217*, 485−500.
(18) Barshilia, H. C.; Ananth, A.; Gupta, N.; Anandan, C. Superhydrophobic Nanostructured Kapton® Surfaces Fabricated through Ar+O2 Plasma Treatment: Effects of Different Environments on Wetting Behaviour. *Appl. Surf. Sci.* **2013**, *268*, 464−471.
(19) Zeng, D. W.; Yung, K. C.; Xie, C. S. XPS Investigation of the Chemical Characteristics of Kapton Films Ablated by a Pulsed TEA CO2 Laser. *Surf. Coat. Technol.* **2002**, *153*, 210−216.
(20) Yang, G.; Han, H.; Du, C.; Luo, Z.; Wang, Y. Facile Synthesis of Melamine-Based Porous Polymer Networks and Their Application for Removal of Aqueous Mercury Ions. *Polymer* **2010**, *51*, 6193−6202.
(21) Fan, L. Z.; Qiao, S.; Song, W.; Wu, M.; He, X.; Qu, X. Effects of the Functional Groups on the Electrochemical Properties of Ordered Porous Carbon for Supercapacitors. *Electrochim. Acta* **2013**, *105*, 299−304.
(22) Sroog, C. E. Polyimides. *Macromol. Rev.* **1976**, *11*, 161−208.

DOI: 10.1021/acsmacrolett.8b00680
ACS Macro Lett. 2018, 7, 1480−1485